Marine Pollution Bulletin 110 (2016) 484–492

Contents lists available at ScienceDirect

Marine Pollution Bulletin

journal homepage: www.elsevier.com/locate/marpolbul

Assessing the bio-mitigation effect of integrated multi-trophic aquaculture on marine environment by a numerical approach

Junbo Zhang *, Daisuke Kitazawa

Institute of Industrial Science, the University of Tokyo, Tokyo 153-8505, Japan

ARTICLE INFO

Article history:
Received 24 March 2016
Received in revised form 3 May 2016
Accepted 2 June 2016
Available online 28 June 2016

Keywords:
Integrated multi-trophic aquaculture
IMTA
MEC ocean model
Impact assessment
Bio-mitigation effect

ABSTRACT

With increasing concern over the aquatic environment in marine culture, the integrated multi-trophic aquaculture (IMTA) has received extensive attention in recent years. A three-dimensional numerical ocean model is developed to explore the negative impacts of aquaculture wastes and assess the bio-mitigation effect of IMTA systems on marine environments. Numerical results showed that the concentration of surface phytoplankton could be controlled by planting seaweed (a maximum reduction of 30%), and the percentage change in the improvement of bottom dissolved oxygen concentration increased to 35% at maximum due to the ingestion of organic wastes by sea cucumbers. Numerical simulations indicate that seaweeds need to be harvested in a timely manner for maximal absorption of nutrients, and the initial stocking density of sea cucumbers >3.9 individuals m^{-2} is preferred to further eliminate the organic wastes sinking down to the sea bottom.

1. Introduction

In aquaculture zones, large amounts of wastes are released from fish cages, transported by water flow, and eventually settle on the sea bottom, consequently resulting in deoxygenation of the aquatic environment (Yokoyama, 2002; Troell et al., 2009). With growing concern over the risks of self-pollution in aquaculture, integrated multi-trophic aquaculture (IMTA) has received extensive attention in recent years as an alternative approach to achieve the sustainability of aquaculture. The main concept of IMTA is to recycle wastes as food resources by cocultivating the targeted species with others, which have different feeding habits in different trophic levels (Neori et al., 2004; Yokoyama, 2013; Zhang and Kitazawa, 2015; Zhang et al., 2015).

Two general candidates for cocultivation with the main culture species in IMTA systems are nutrient absorbers and deposit feeders (Troell et al., 2009; Yokoyama and Ishihi, 2010). The nutrient absorbers, such as seaweeds, can absorb and therefore remove the dissolved nutrients produced in fish-farming operations (Chopin et al., 2001; Neori et al., 2004; Buschmann et al., 2008; Yokoyama and Ishihi, 2010). The deposit feeders, for example, sea cucumbers, ingest substantial amounts of organic wastes from the surface layer of bottom sediments, thereby reducing the content of organic wastes in sediments (Kitano et al., 2003; Ren et al., 2010). When the nutrients released from fish-farming operations are fully balanced by the harvest of the extractive components such as seaweeds, mussels, and sea cucumbers, the IMTA system can create the maximum benefit in the aspects of both environment and economy (Troell et al., 2009). Matter and energy flux within IMTA, and between IMTA and its surrounding environment need to be qualified and quantified, to assess the bio-mitigation effect of IMTA and investigate its optimal design, so that the sustainability of aquaculture can be achieved (Reid et al., 2009; Chopin et al., 2013).

Nevertheless, the high complexity of an IMTA system may complicate the assessment of its bio-mitigation effect through the traditional technique of trials and small-scale experiments (Troell et al., 2009; Ren et al., 2012). To some degree, a mathematical model is a potential tool to evaluate the overall bio-mitigation effect of an IMTA system and facilitate an understanding of the interactions among physical, biochemical, and hydrodynamic characteristics in an IMTA system (Reid, 2011).

The purpose of this study is to explore the negative impacts of aquaculture wastes and assess the bio-mitigation effect of IMTA systems on marine environments by a three-dimensional (3D) numerical simulation approach. The original Marine Environmental Committee (MEC) ocean model was composed of physical and ecosystem submodels (Kitazawa, 2001; Sato et al., 2006; Mizumukai et al., 2008; Kitazawa and Yang, 2012). The model was recently developed by considering the drag of fish cages and the diffusion of particulate organic waste submodels by Zhang and Kitazawa (2015). In this study, the extended MEC ocean model was further improved by coupling the seaweed *Ulva ohnoi* and the sea cucumber *Apostichopus japonicus* submodels to represent the ecological processes in IMTA systems. The seaweed submodel in this study follows the previous works (e.g. Solidoro et al., 1997; Ren et al., 2012), while the submodel of sea cucumbers is originally developed by the authors based on the theory of scope for growth.

* Corresponding author.
E-mail addresses: zjb@iis.u-tokyo.ac.jp, zhangjunbo1985@gmail.com (J. Zhang).

http://dx.doi.org/10.1016/j.marpolbul.2016.06.005
0025-326X/

2. Materials and methods

2.1. Study area

Gokasho Bay is a typical marine embayment in Japan. With the development of fish farming over the last several decades, the surrounding marine environment has become severely degraded, especially in Hazama-ura area (Fig. 1), because of the large amount of wastes produced by mariculture operations (Yokoyama, 2002; Yokoyama et al., 2009). With great concerns over the seasonal deoxygenation of bottom water, a small-scale IMTA trial was conducted in Gokasho Bay, where the Japanese sea cucumber *A. japonicus* and the seaweed *U. ohnoi* were cocultured (Yokoyama and Ishihi, 2010; Yokoyama, 2013; Zhang et al., 2015).

The stations for data monitoring are also represented in Fig. 1. The observation data of dissolved inorganic nitrogen (DIN) and phosphorus in station A at 2 m below sea surface were monitored by the National Institute for Environmental Studies, Japan. The data of water temperature, phytoplankton, and dissolved oxygen (DO) in station B were observed by Mie Prefecture Fisheries Research Institute (Japan) at 0.5 m below sea surface and 0.5 m above sea bottom.

2.2. Numerical model

On the basis of hydrostatic and Boussinesq assumptions, the governing equations of physical component in MEC ocean model basically consist of the equation of continuity, 3D Reynolds-averaged Navier–Stokes (RANS) equations, advection–diffusion equations of water temperature and salinity, and the equation of state. The eddy viscosity and diffusivity coefficients are given as constant values or calculated from stratification functions. The effect of fish cages is added to the RANS equations (Zhang and Kitazawa, 2015).

Up to 15 state variables are generally formulated in the numerical model to reproduce the complex processes of material cycling in an IMTA system (Fig. 2). The primary production process is controlled by phosphorus and nitrogen, because phytoplankton and seaweed generally experience these two nutrient sources as the possible limitation factors. The species of phytoplankton or zooplankton are summarized by one state variable for simplicity. Particulate organic carbon is composed of three sources: the feces of zooplankton and sea cucumber, the death of organisms, and the bacteria. After particulate organic wastes sink down to the sea bottom, a fraction of them are resuspended as the particulate organic carbon. The detritus from seaweeds is also one of the

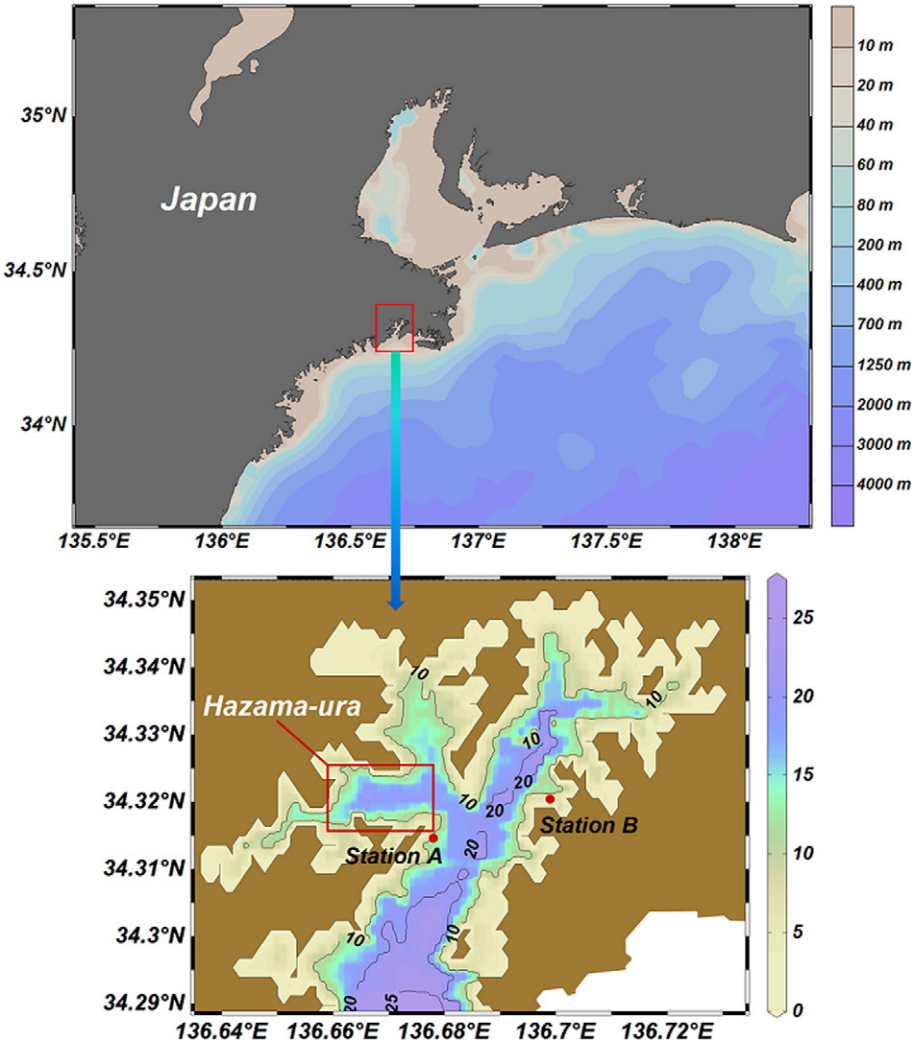

Fig. 1. Map of the study area. The red rectangle shows the location of the fish farm in the Hazama-ura area, Japan, and the red dots denote the stations A and B where data on water temperature, nutrients, phytoplankton, and dissolved oxygen are observed.

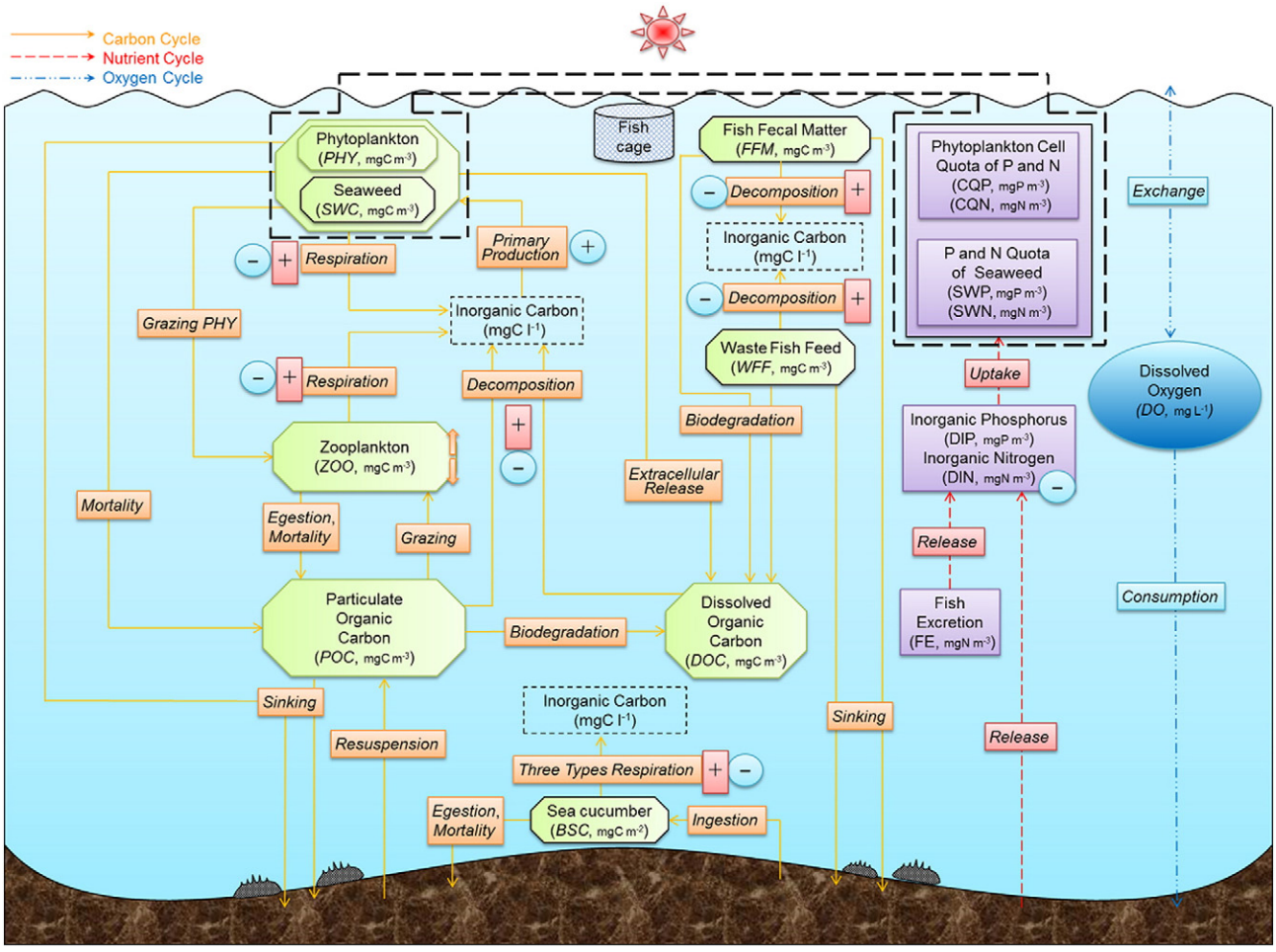

Fig. 2. Numerical ecological processes of each component in an integrated multi-trophic aquaculture system in this study. Boxes and arrows represent state variables and fluxes, respectively. ⊕ indicates nutrients are produced through the associated process. ⊕ indicates the dissolved oxygen is produced through the associated process. ⊖ indicates the dissolved oxygen is consumed through the associated process. ⊕ denotes the migration of zooplankton.

contributors of particulate organic carbon. However, the amount of particulate organic carbon decreased due to the ingestion of sea cucumbers. Extracellular release of phytoplankton and seaweed, as well as a fraction of production from bacterial decomposition of particulate organic carbon and aquaculture organic wastes, comprise the dynamic process of dissolved organic carbon, although it is refractory and its decomposition rate is much lower than that of particulate organic carbon. The processes involved in the DO cycles, that is, oxygen exchange at the air–water interface, production via photosynthesis process in the euphotic zone and consumption due to respiration, and organic matter oxidation in the entire water column, are modeled. A microbial loop is not taken into consideration and bacteria are not selected as a state variable, while their roles in the decomposition process of organic carbon are implicitly taken into account by release of nutrients and consumption of DO.

Chemical materials, planktons, and aquaculture wastes are assumed to be transported by the surrounding water flow. Their dynamics can be described by the advection–diffusion equation as follows:

$$\frac{\partial E_{co}}{\partial t}+\frac{\partial(uE_{co})}{\partial x}+\frac{\partial(vE_{co})}{\partial y}+\frac{\partial(wE_{co})}{\partial z} = \frac{\partial}{\partial x}\left(A_H\frac{\partial E_{co}}{\partial x}\right)+\frac{\partial}{\partial y}\left(A_H\frac{\partial E_{co}}{\partial y}\right)+\frac{\partial}{\partial z}\left(K_H\frac{\partial E_{co}}{\partial z}\right)+q_{E_{co}} \quad (1)$$

where t is time (s); u, v, and w are water current velocities in x, y, and z directions (m s^{-1}), respectively; E_{co} represents each state variable; $q_{E_{co}}$ denotes the time change in each state variable due to chemical–biological processes; A_H is the horizontal eddy diffusivity coefficient (10 for a 1000-m mesh, m^2 s^{-1}) (Yanagi, 2000); and K_H is the vertical eddy diffusivity coefficient (m^2 s^{-1}). The horizontal eddy diffusivity coefficients were low before the advent of numerical instability, that is, in the range of the results of diffusion experiments (Okubo, 1975, 1976; List et al., 1990).

The mathematical model for seaweed is developed based on the existing models of Solidoro et al. (1997) and Ren et al. (2012). Three state variables are considered in seaweed submodel: seaweed (*SWC*, mgC m^{-3}), DIN quota of seaweed (*SWN*, mgN m^{-3}), and dissolved inorganic phosphorus quota of seaweed (*SWP*, mgP m^{-3}). Nitrogen is the main nutrient that controls seaweed growth. Phosphorus and silicon are not relevant in most environments (Sfriso et al., 1989; Solidoro et al., 1997; Ren et al., 2012). However, phosphorus is taken into account to maintain a general formulation, considering the potential competition of phosphorus between seaweed and phytoplankton (Coffaro and Sfriso, 1997). In general, silicon is ignored in the seaweed submodel, because it usually does not become the limiting factor. The state equations are described as follows:

$$\frac{\partial SWC}{\partial t}=P_{gswc}-P_{erswc}-P_{rswc}-P_{mswc} \quad (2)$$

$$\frac{\partial SWP}{\partial t}=P_{po4usw}-[P:C]_{sw}P_{gswc}-P_{mswc}\frac{SWP}{SWC} \quad (3)$$

$$\frac{\partial SWN}{\partial t} = P_{nh4usw} + P_{no3usw} - [N:C]_{sw} P_{gswc} - P_{mswc} \frac{SWN}{SWC} \quad (4)$$

where P_{gswc} is the process of seaweed growth (mgC m^{-3} d^{-1}), P_{erswc} is the process of extracellular release by seaweed (mgC m^{-3} d^{-1}), P_{rswc} is the process of seaweed respiration (mgC m^{-3} d^{-1}), P_{mswc} is the process of seaweed mortality (mgC m^{-3} d^{-1}), P_{po4usw} is the process of phosphate uptake by seaweed (mgP m^{-3} d^{-1}), $[P:C]_{sw}$ is the ratio of phosphorus to carbon (0.04, –), P_{nh4usw} is the process of ammonium uptake by seaweed (mgN m^{-3} d^{-1}), P_{no3usw} is the process of nitrate uptake by seaweed (mgN m^{-3} d^{-1}), and $[N:C]_{sw}$ is the ratio of nitrogen to carbon (0.1, –) (Ren et al., 2012).

The biomass of sea cucumbers in terms of carbon (*BSC*, gC m^{-2}) can be calculated by multiplying the population density of sea cucumbers (N_{sc}, –) by the average body weight of an individual sea cucumber (*BMSC*, g) and the conversion coefficient of carbon to wet body weight of sea cucumbers ($[C:BM]_{sc}$, 0.3, –). The mortality process of sea cucumbers (P_{msc}, mgC m^{-2} d^{-1}) is also considered as the biomass loss term. The dynamic change of *A. japonicus* biomass in an area of computational grid (A_{reasc}, 1.82×10^4, m^2) is therefore described as

$$\frac{\partial BSC}{\partial t} = \frac{Nsc \cdot [C:BM]_{sc}}{Areasc} \frac{\partial BMSC}{\partial t} - P_{msc} \quad (5)$$

$$\frac{\partial BMSC}{\partial t} = (P_{sigsc} - P_{aexsc}) \cdot C_{ccisc} - P_{arsc} - P_{sdarsc} - P_{srsc} \quad (6)$$

where P_{sigsc}, P_{aexsc}, P_{arsc}, P_{sdarsc}, and P_{srsc} represent the processes of food ingestion, digestion/excretion, active respiration, specific dynamic action respiration, and standard respiration (g d^{-1}), respectively, and C_{ccisc} is the conversion coefficient of organic matter to body mass of sea cucumbers (1.75, –) (Zhang, 2014).

2.3. Boundary conditions

In general, the boundary conditions at the sea surface are composed of the dynamic boundary condition; kinematic boundary condition; wind friction condition; and fluxes of heat, salt, and biochemical materials. The surface wind stress is for the momentum equations and the surface heat flux is for the temperature equation, which is composed of short-wave solar radiation (Q_{Swsr}, J m^{-2} s^{-1}), net long-wave radiation (Q_{Lwr}, J m^{-2} s^{-1}), sensible heat transport due to convection (Q_{hc}, J m^{-2} s^{-1}), and latent heat transport due to evaporation (Q_{eva}, J m^{-2} s^{-1}). The effective surface salt flux is for the salinity equation. The bottom boundary conditions include kinematic boundary condition; fluxes of heat, salt, and chemical materials; and bottom friction condition. The bottom frictional stresses are for the momentum equations. It is assumed that there are neither advective nor diffusive fluxes of heat and salt across the sidewalls. Hence, the normal gradients of water temperature and salinity are zero on the sidewalls. Current velocity component normal to the walls is zero, while the free-slip condition is applied to the velocity component parallel to the walls. Both surface wind stress and bottom frictional stresses can be formulized and parameterized by a quadratic drag law. The formulation and parameters of boundary conditions are represented in Tables 1 and 2, respectively.

2.4. Computational conditions

Numerical simulation was conducted for 6 months from 21 August 2009 to obtain data on variations in water temperature, salinity, current velocity, and state variables. Meteorological data recorded around Gokasho Bay (provided by the Japan Meteorological Agency) were reviewed to estimate heat and salt fluxes through the water surface. These included atmospheric temperature, atmospheric pressure, solar radiation, amount of cloud, relative humidity, precipitation, and wind velocity and direction as measured in the field. Water level elevation due to tide is observed in the Gokasho Bay by the Hydrographic and Oceanographic Department of the Japan Coast Guard. A total of eight tidal components were forced in the nonflection scheme at the open boundary (Hino and Nakaze, 1989).

We conducted a total of four simulation scenarios as described in Table 3. The initial values of wastes for Scenarios 2–4 were set as 234 gC m^{-2} d^{-1} and 34 gN m^{-2} d^{-1} in Hazama-ura fish farm during April (Yokoyama et al., 2006). Seaweeds were planted around each fish cage, and sea cucumbers were cultured at the sea floor just beneath fish cages. The initial biomass of seaweeds for Scenarios 3 and 4 is represented in Fig. 3a, the initial density of sea cucumbers for Scenario 3 is shown in Fig. 3b, and that for Scenario 4 is represented in Fig. 3c. The initial body weight of sea cucumbers for both Scenarios 3 and 4 was set at 10 g.

2.5. Computational method

The computational domain is Gokasho Bay (Fig. 1). It was latticed by a square grid of 135 m in the horizontal direction. The thickness of the grids was 1 m in the vertical direction, while the last two grids above water bottom were given a thickness of 2 m. A staggered grid system was adopted at each mesh to arrange the evaluation points of current velocity, pressure, water temperature, salinity, density, and state

Table 1
Formulation of boundary conditions at sea surface and sea bottom.

Boundary	Formulation
Sea surface $z=\xi(m)$	$p = p_a$ $-\frac{\partial \xi}{\partial t} - u\frac{\partial \xi}{\partial x} - v\frac{\partial \xi}{\partial y} + w = 0$ $\tau_x = C_d \rho_a W_x \sqrt{{W_x}^2 + {W_y}^2}$, $\tau_y = C_d \rho_a W_y \sqrt{{W_x}^2 + {W_y}^2}$ $\rho_a = 1.293 \frac{273.15 p_a (1 - 0.378 E_a / p_a)}{(273.15 + T_a) \cdot 1013.25}$, $E_a = E_s \cdot h$, $E_s = 6.1078 \times 10^{7.5 T_a / (273.3 + T_a)}$ $K_M \frac{\partial u}{\partial z} = \frac{\tau_x}{\rho_0}$, $K_M \frac{\partial v}{\partial z} = \frac{\tau_y}{\rho_0}$, $K_H \frac{\partial T}{\partial z} = \frac{Q_{Temp}}{\rho_0 C_P}$, $K_H \frac{\partial S}{\partial z} = \frac{Q_{Salt}}{\rho_0}$, $K_H \frac{\partial E_{co}}{\partial z} = 0$
Surface salt flux	$Q_{Salt} = S \cdot \{\rho_a C_E (q_s - q_a) W - P_r\}$ $q_s = \frac{0.622 E_s}{p_a - 0.378 E_s}$, $q_a = \frac{0.622 E_a}{p_a - 0.378 E_a}$
Surface heat flux	$Q_{Temp} = Q_{Swsr} + Q_{Lwr} + Q_{hc} + Q_{eva}$ $Q_{Swsr} = Q_{s0}(1 - ref.)$, $Q(z) = Q_{s0} \exp(k_{ex} \cdot z)$ $Q_{Lwr} = s\sigma(T_a + 273.15)^4 (0.39 - 5.8 \times 10^{-2} \sqrt{E_a})(1 - cC^2) + 4s\sigma(T_a + 273.15)^3 (T - T_a)$ $Q_{hc} = C_a \rho_a C_H (T - T_a) W$ $Q_{eva} = L \rho_a C_E (q_s - q_a) W$
Sea bottom $z = -H(m)$	$u\frac{\partial H}{\partial x} + v\frac{\partial H}{\partial y} + w = 0$ $\tau_{xB} = \gamma^2 \rho_0 u \sqrt{u^2 + v^2}$, $\tau_{yB} = \gamma^2 \rho_0 v \sqrt{u^2 + v^2}$ $K_M \frac{\partial u}{\partial z} = \frac{\tau_{xB}}{\rho_0}$, $K_M \frac{\partial v}{\partial z} = \frac{\tau_{yB}}{\rho_0}$, $K_H \frac{\partial T}{\partial z} = 0$, $K_H \frac{\partial S}{\partial z} = 0$, $K_H \frac{\partial E_{co}}{\partial z} = 0$

Table 2
Definition of variables and parameters for boundary condition.

Definition	Symbol	Value and unit
Amplitude of tide	ξ	m
Pressure	p	N m^{-2}
Atmospheric pressure	p_a	N m^{-2}
Surface frictional stress caused by wind in x direction	τ_x	N m^{-2}
Surface frictional stress caused by wind in y direction	τ_y	N m^{-2}
Wind friction coefficient	C_d	–
Density of air	ρ_a	kg m^{-3}
Wind velocity in x direction	W_x	m s^{-1}
Wind velocity in y direction	W_y	m s^{-1}
Vapor pressure	E_a	hPa
Atmospheric temperature	T_a	°C
Water temperature	T	°C
Saturated vapor pressure	E_s	hPa
Vertical eddy viscosity coefficient	K_M	m^{-2} s^{-1}
Salinity	S	psu
Relative humidity	h	–
Heat flux through sea surface	Q_{Temp}	J m^{-2} s^{-1}
Salt flux through sea surface	Q_{Salt}	kg m^{-2} s^{-1}
Specific heat of water	C_P	4080, J kg^{-1} K^{-1} (Kondo, 1994)
Bulk coefficient of latent heat transport	C_E	–
Saturated specific humidity	q_s	–
Specific humidity	q_a	–
Wind velocity	W	m s^{-1}
Atmospheric precipitation	P_r	kg m^{-2} s^{-1}
Global solar radiation	Q_{s0}	J m^{-2} s^{-1}
Albedo at sea surface	ref.	0.09, – (Kondo, 1994)
Emissivity	s	0.96, – (Kondo, 1994)
Stefan–Boltzmann constant	σ	5.67×10^{-8}, W m^{-2} K^{-4} (Kondo, 1994)
Cloud coefficient	c	0.65, – (Hirose et al., 1996)
Amount of cloud	C	
Specific heat of air	C_a	1.01×10^3, J kg^{-1} K^{-1} (Kondo, 1994)
Bulk coefficient of sensible heat transport	C_H	–
Latent heat of evaporation	L	2.45×10^6, J kg^{-1} (Kondo, 1994)
Extinction coefficient of light	k_{ex}	0.1, m^{-1}
Bottom frictional stress in x direction	τ_{xB}	N m^{-2}
Bottom frictional stress in y direction	τ_{yB}	N m^{-2}
Friction coefficient	γ^2	2.6×10^{-3}, – (Unoki, 1993)
Reference density of water	ρ_0	1025, kg m^{-3}

variables. After the input of computational conditions, water surface elevation, horizontal and vertical current velocities, water temperature, salinity, density, and state variables were calculated.

Finite difference methods were applied to the governing equations. The explicit time integration method of Euler was used for time-derivative terms. The quadratic upstream interpolation for convective kinematics (QUICK) was applied to convection or advection terms. The eddy viscosity or diffusivity terms were solved by second-order central difference method. Time step was set at 5 s for the simulation of current velocity, and 60 s for water temperature, salinity, and state variables. Ocean Data View (V4.5.3) (Schlitzer, 2013) and R® (R Development Core Team, 3.0.0 for Windows) were adopted for data visualization.

Table 3
Description of four-scenario simulations in this study.

Scenario simulation	Description	Element		
		Wastes	Seaweed	Sea cucumber
Scenario 1	Reference environment	–	–	–
Scenario 2	Impact of aquaculture wastes	✓	–	–
Scenario 3	Bio-mitigation of IMTA	✓	✓	✓
Scenario 4	Effect of initial density of sea cucumbers	✓	✓	✓

3. Results and discussion

3.1. Model validation

In general, it is difficult to observe phytoplankton individually with the naked eye due to its extremely small size. However, the biomass of phytoplankton can be determined by using chlorophyll-*a* in phytoplankton cells, which will appear as a discoloration of the water. Therefore, the concentration of chlorophyll-*a* is an appropriate indicator to present the dynamics of phytoplankton concentration (Kitazawa, 2001). The changes in the concentrations of observed chlorophyll-*a* at 0.5 m below the sea surface are represented in Fig. 4a. In general, the blooms of diatom, dinoflagellate, and green algae in a lake could cause the peaks to occur during spring and summer (Kitazawa et al., 2010). However, in the open sea, phytoplankton is not abundant during summer due to limited nutrients. Two peaks of chlorophyll-*a* concentration can be observed at the end of July and the beginning of October, because nutrient enrichment in the water column, such as DIN and dissolved inorganic phosphorus (DIP), occurs during warm period (Fig. 4b and 4c). In Gokasho Bay, blooms of dinoflagellate have been observed during summer season (Uchida et al., 1998). The algal bloom at the beginning of August could be reproduced well by our model. However, the peak of chlorophyll-a observed in October is underestimated in the simulation. The blooms of algae during autumn may be caused by cyanobacteria (Kitazawa et al., 2010). In general, the photosynthetic growth of phytoplankton shows a positive relationship with increased water temperature until a species-specific maximum is reached, if the light intensity and nutrients are not limited (Eppley, 1972). Although the general water temperature effect is considered in our model, different species of phytoplankton require various optimal water temperatures for growth. The current model did not consider the difference among the phytoplankton species, which may produce the discrepancy between observation and simulation results of phytoplankton concentration.

The bottom DO decreased gradually from April to the beginning of October (Fig. 4d). It might be caused by the stratification of water temperature. The increase in surface water temperature started from the beginning of seasonal warming and its rising speed was higher than that at the sea bottom from May to September (Fig. 5). The DO concentration at sea surface was saturated by the exchange at the air–sea interface and the primary producers, and then transported to bottom layers. When the water temperature started stratifying, it may have led to a hypoxic condition due to obstruction in transportation of DO from the surface to the bottom. Such variations in water temperature and DO were reproduced by the model successfully.

3.2. Impact of aquaculture wastes

After the aquaculture wastes were released from fish farms in the Hazama-ura area, the concentration of DIN increased significantly from the fish farm to the inner part of the Hazama-ura area, and the diffusion of DIN covered almost the entire bay (Fig. 6). Risks of eutrophication and harmful algal blooms will be increased near the coastal line, especially around the inner part of the Hazama-ura area with a high concentration of DIN.

The concentration of bottom DO in Gokasho Bay is presented in Fig. 6. Yokoyama et al. (2006) investigated the distribution of DO concentration in the Hazama-ura fish farm and found that the area with <1 mg l^{-1} of DO extended over the fish farm area, especially in the area between the northern and southern cage rows and toward the inner part of the Hazama-ura area. Our simulation results reproduced their findings well. The decrement of bottom DO was attributed to the higher consumption of oxygen in the decomposition process of the organic wastes, which was released from fish farms and sank down to the sea bottom. In general, if the nonaquaculture-derived nitrogen increases, the DO in the water near the surface of sediment decreases linearly in natural

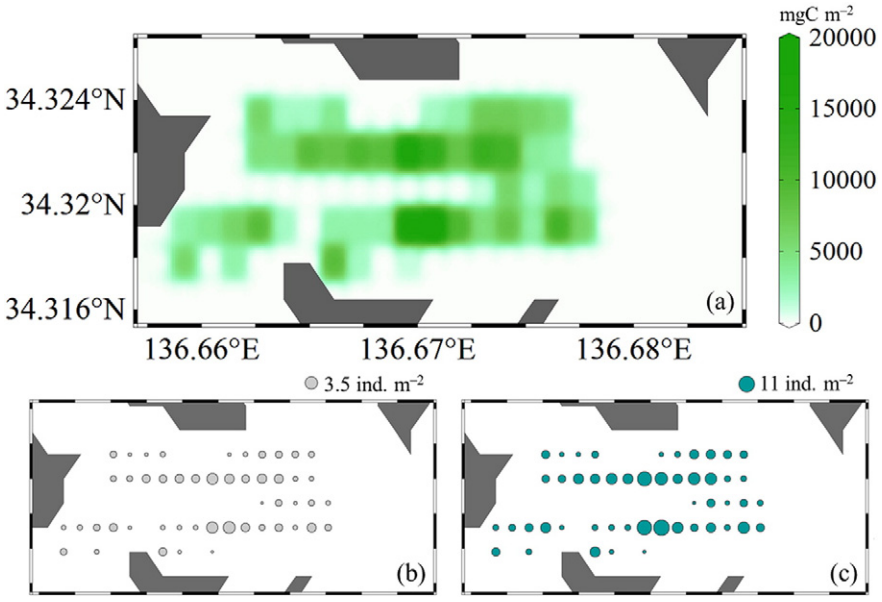

Fig. 3. (a) Initial biomass of seaweeds for Scenarios 3 and 4, (b) Initial density of sea cucumbers for Scenario 3, (c) Initial density of sea cucumbers for Scenario 4, in each computational grid.

environment; however, it declines logarithmically as the aquaculture wastes increase (Yokoyama et al., 2006). An obvious decrement of bottom DO concentration can be also found nearby fish farm in the simulation, when the aquaculture wastes load on the sea bottom. Yokoyama et al. (2006) reported that organic waste content decreased with an increasing distance from the fish cages, and an anoxic state of the waters was found when the waste content in sediment was as high as 2 mg g^{-1} in the Hazama-ura area. They also found that the enrichment effects on the bottom water and sediment chemistry extended to a much larger area than the waste dispersal area. The low concentration of DO can still be observed even in areas at a distance of more than 300 m from fish farms in our numerical simulation, indicating a rather severe degradation of bottom water in Gokasho Bay. Thus, in order to achieve the objective of sustainable aquaculture and reduce the negative impacts of aquaculture wastes, IMTA systems should be applied to the Hazama-ura area.

3.3. Bio-mitigation effect of IMTA

Because only limited information on the bio-mitigation effect of IMTA (Yokoyama, 2013) is available, an assessment is urgently needed to understand how aquatic environments are improved with IMTA systems. In this study, our simulation results might serve as an evaluation of the mitigation effects of IMTA on marine environments.

Figure 7 represents the percentage change in concentrations of phytoplankton, nitrate, and DO near sea surface and sea bottom after the application of IMTA. Near the sea surface, the concentration of phytoplankton deceased sharply in the Hazama-ura fish farm by a maximum

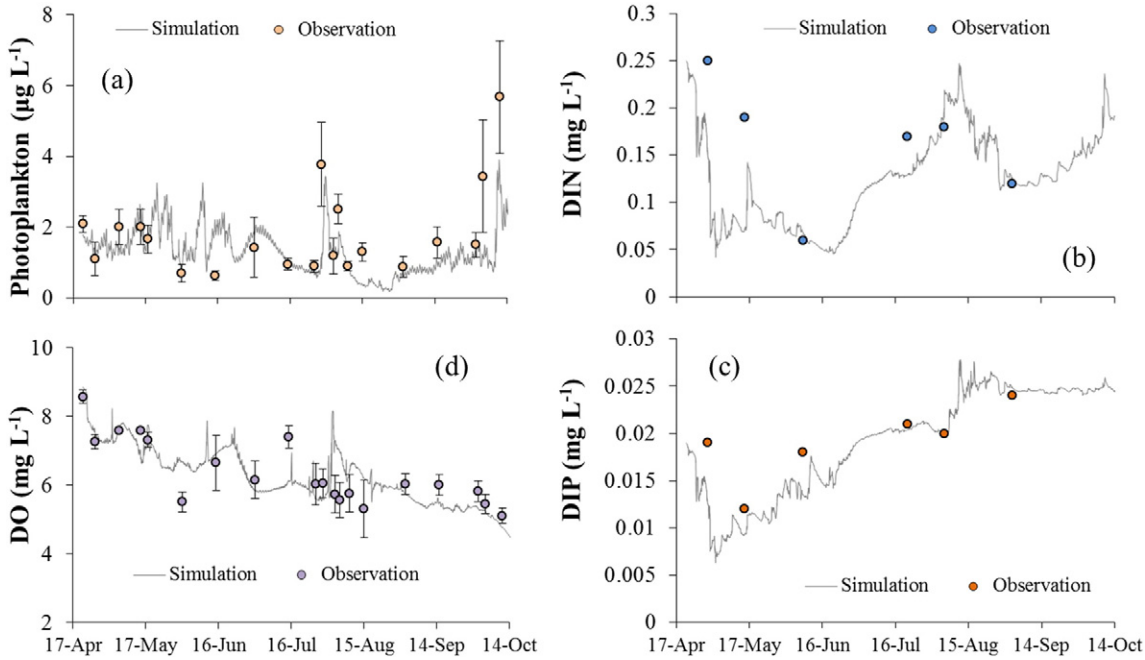

Fig. 4. Observation and simulation of (a) surface phytoplankton, (b) surface dissolved inorganic nitrogen, (c) surface dissolved inorganic phosphorus, and (d) bottom dissolved oxygen.

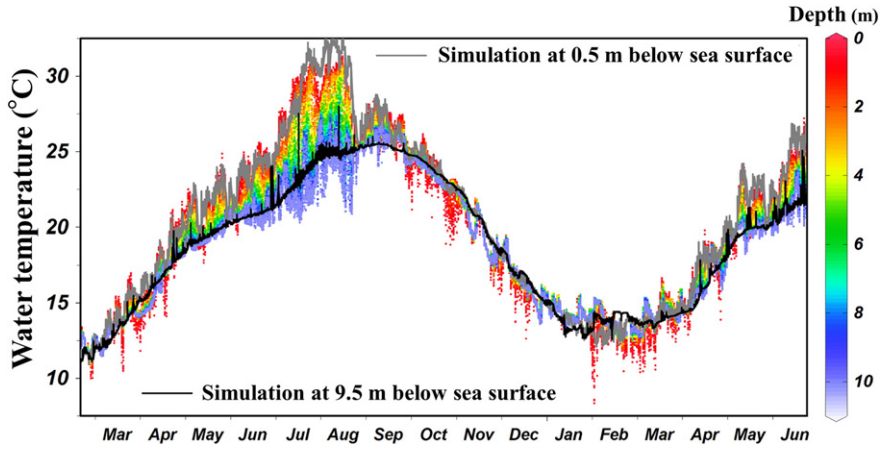

Fig. 5. Observation and simulation of water temperature.

of 30%. A possible explanation for the acute reduction of phytoplankton is that seaweeds blocked sunlight through their blades spreading over the sea surface. Insufficient light intensity in the areas where seaweeds were cultured led to the limited growth of phytoplankton. This may indicate that seaweeds in IMTA systems affect the concentration of phytoplankton more through the shading effect than the competition effect of nutrients, especially when nutrients are sufficiently supplied. In contrast to the acute decrease of phytoplankton, a slight reduction in the nitrate concentration could be found (Fig. 7). Cubillo et al. (2016) also observed that, although the added nitrogen resulted in a 22% increment in the production of winged kelp *Alaria esculenta*, there was no significant decrease in ambient nutrient concentration in IMTA systems. The main reason for this phenomenon is the slowdown of nutrient uptake after seaweeds absorb the maximum level of nutrients into their bodies. This indicates that timely harvest of seaweeds in the practice of IMTA will help realize more efficient utilization of nitrogen. In our simulation, the process of seaweed harvest was not considered into the model, which may explain the small changes in the reduction of nutrient concentration. With respect to DO, an increased concentration was observed on the sea surface surrounding the fish farms. This can be attributed to the higher photosynthetic capacity of seaweeds than phytoplankton. Simulation results at the sea surface indicate that the aquatic environment around the fish cages could be improved when the nutrient absorber seaweed is cocultured in IMTA systems.

The percentage change in the concentration of phytoplankton near the sea bottom after the application of IMTA displayed a maximum

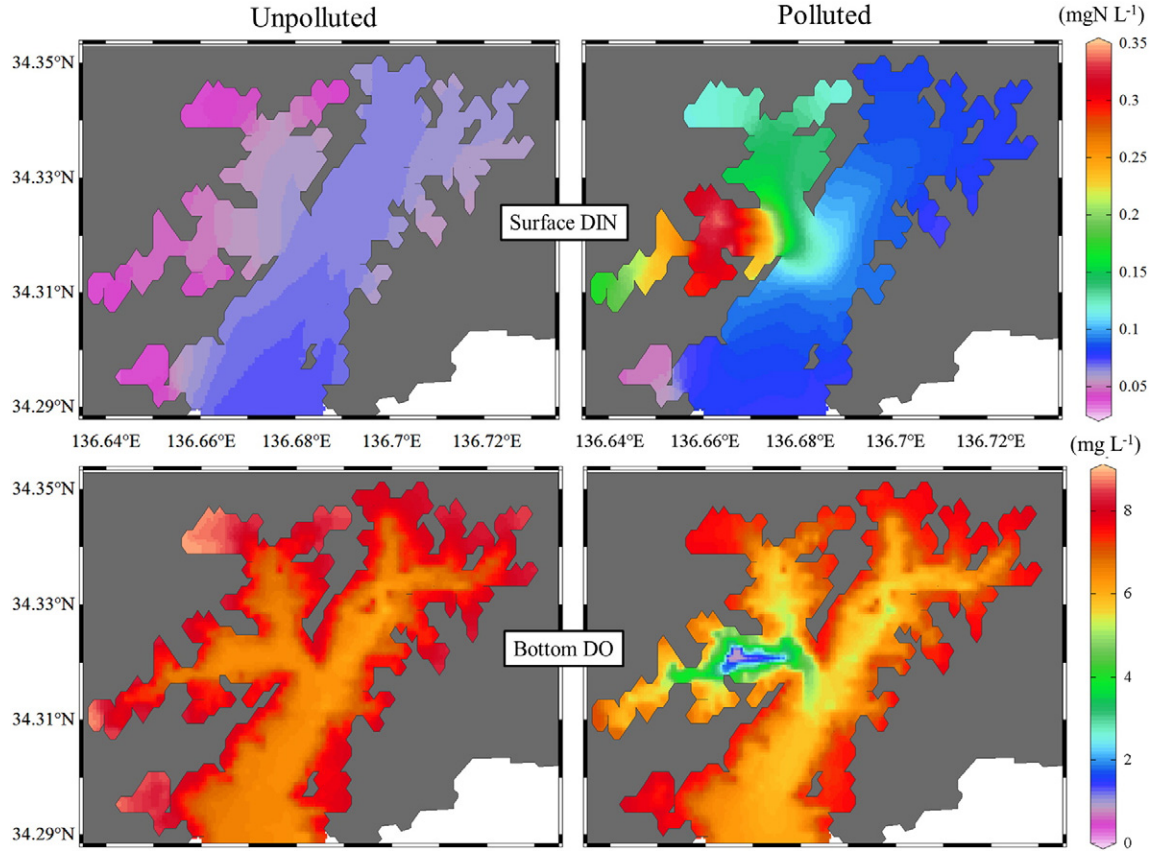

Fig. 6. Monthly mean concentrations of dissolved inorganic nitrogen (DIN) near sea surface and dissolved oxygen (DO) near sea bottom without (left) and with (right) aquaculture wastes.

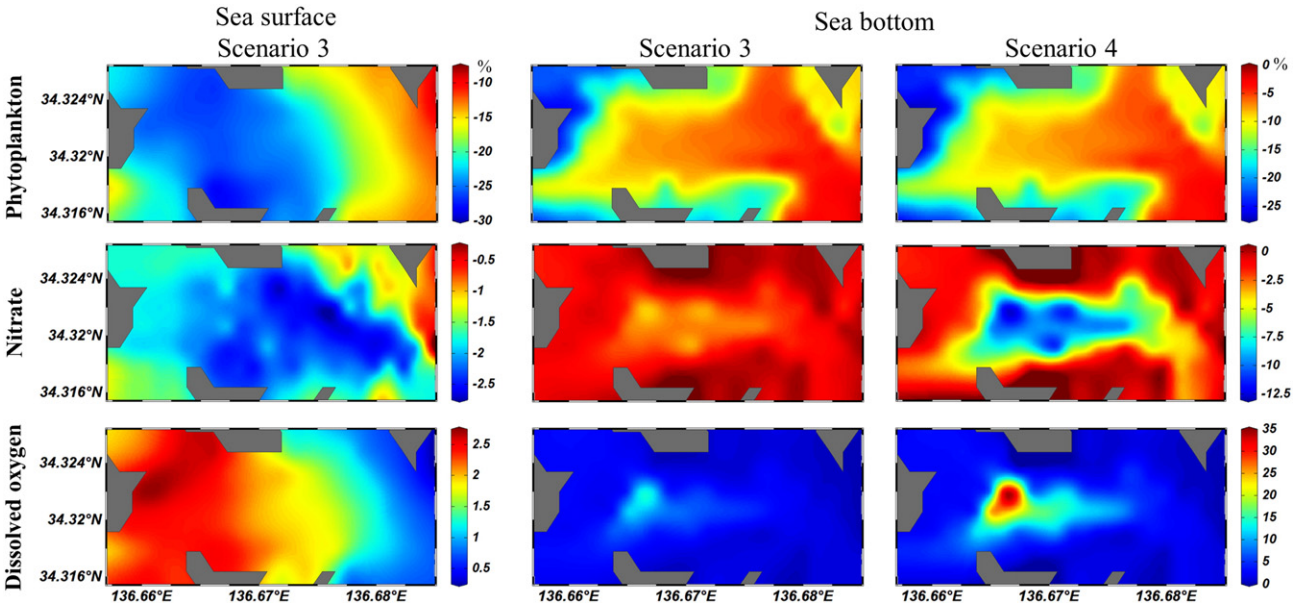

Fig. 7. Percentage change in concentration of phytoplankton, nitrate, and dissolved oxygen near sea surface and sea bottom after the application of IMTA.

reduction of 25% (Fig. 7), which was supposed to be caused by the reduced amount of phytoplankton sinking from the sea surface. The concentration of DIN at the sea bottom also showed a decrease, while bottom DO concentration with a range of 5–15% improvement could be found after the IMTA system was carried out, as represented in Fig. 7. This can be explained by the corresponding decrease in organic waste content in sediment. The uptake of bottom sediments by sea cucumbers reduces the release of nutrients and brings about the decrease in the consumption of bottom DO. This proves the capacity of sea cucumbers to improve the marine environment and its importance in IMTA systems.

3.4. Effect of initial density of sea cucumbers

In Scenario 3, where the mean initial density of sea cucumbers was 1.2 ind. m^{-2}, the capacity of sea cucumbers to improve the aquatic environment near the sea bottom by ingesting particulate organic wastes was proven by our simulation results. In Scenario 4, where the mean initial stocking density was increased to 3.9 ind. m^{-2}, the percentage change in nitrate reduction increased to 12.5% at maximum, and the percentage change in the improvement of DO concentration was further increased to 35%. This corresponds well with the result of Li et al. (2014), who suggested that a higher stocking density of sea cucumbers might be preferred in the field investigation of IMTA systems. They reported that although the total organic carbon in sediments could be removed by sea cucumbers when the stocking density was 2 ind. m^{-2} (body mass 9 g), the ratio of organic matter in the sediment increased persistently during the whole culture period. Hence, they proposed an increase in the initial density of sea cucumbers, which could probably further increase the rate of utilization of organic carbon in IMTA systems. Our simulation results supported their viewpoint in this aspect. Nevertheless, although the density in this study (3.9 ind. m^{-2}) was higher than that reported by Li et al. (2014), a low DO concentration (<1 mg l^{-1}) could still be observed, implying that a further higher initial density of sea cucumbers is required, to sufficiently eliminate the organic waste loading on the sea bottom.

4. Conclusions

On the basis of the improved MEC ocean model, numerical simulations were performed to assess the bio-mitigation effect of IMTA system on marine environment. The mitigation effect was evaluated through the changes in the concentrations of phytoplankton, DIN, and DO. A total of four scenarios were adopted in this study. Scenario 1 functioned as the reference simulation. Scenario 2 was conducted to investigate the negative effects of fish-farming operations on the local aquatic environment before the implementation of IMTA. In scenarios 3, an IMTA system was implemented, where seaweeds and sea cucumbers were cocultured to assess the bio-mitigation effect of IMTA systems. In scenario 4, the density of sea cucumbers was increased to understand the effect of the initial density of sea cucumbers on bio-mitigation.

Simulation results showed that the aquatic environment in Gokasho Bay deteriorated rapidly when the aquaculture wastes were released from fish farms. The dissolved nutrients increased in the water from the sea surface to bottom, and the bottom DO deceased to approximately 0 mg l^{-1} in the Hazama-ura area. After the application of IMTA, the aquatic environment was improved by planting seaweeds at the upper layer near the sea surface and releasing sea cucumbers on the sea floor. The concentration of phytoplankton could be controlled by planting seaweed, and that of bottom DO increased due to the ingestion of organic wastes by sea cucumbers. Moreover, a higher initial density of sea cucumbers could further mitigate the deterioration of water environment near the sea bottom.

Numerical simulations indicated that seaweeds need to be harvested on time to absorb the nutrients maximally; further, an initial stocking density of sea cucumbers >3.9 ind. m^{-2} is preferred to further eliminate the organic wastes sinking down to the bottom.

In future studies, frequency and time for seaweed harvest need to be considered in the numerical model, and the optimal density for stocking sea cucumbers as well as their initial body weight should be investigated. Furthermore, the survival rate of sea cucumbers in hypoxic environment is also a key issue to be included in future studies.

Acknowledgments

This study was partly supported by Society for Conservation of Fisheries Resources and Marine Environment (CoFRaME). The authors are grateful to Prof. Yokoyama for his valuable comments on this study. We would like to thank Japan National Institute for Environmental Studies and Mie Prefecture Fisheries Research Institute for providing the precious observed data of water quality, as well as Japan

Meteorological Agency and Japan Coast Guard for providing the meteorological and tidal level data, respectively.

References

Buschmann, A.H., Varela, D.A., Hernández-González, M.C., Huovinen, P., 2008. Opportunities and challenges for the development of an integrated seaweed-based aquaculture activity in Chile: determining the physiological capabilities of *Macrocystis* and *Gracilaria* as biofilters. J. Appl. Phycol. 20, 571–577.

Chopin, T., Buschmann, A.H., Halling, C., Troell, M., Kautsky, N., Neori, A., Kraemer, G.P., Zertuche-González, J.A., Yarish, C., Neefus, C., 2001. Integrating seaweeds into marine aquaculture systems: a key toward sustainability. J. Phycol. 37, 975–986.

Chopin, T., MacDonald, B., Robinson, S., Cross, S., Pearce, C., Knowler, D., Noce, A., Reid, G., Cooper, A., Speare, D., Burridge, L., Crawford, C., Sawhney, M., Ang, P.K., Backman, C., Hutchinson, M., 2013. The Canadian integrated multi-trophic aquaculture network (CIMTAN)—a network for a new era of ecosystem responsible aquaculture. Fisheries 38 (7), 297–308.

Coffaro, G., Sfriso, A., 1997. Simulation model of *Ulva rigida* growth in shallow water of the Lagoon of Venice. Ecol. Model. 102 (1), 55–66.

Cubillo, A.M., Ferreira, J.G., Robinson, S.M., Pearce, C.M., Corner, R.A., Johansen, J., 2016. Role of deposit feeders in integrated multi-trophic aquaculture—a model analysis. Aquaculture 453, 54–66.

Eppley, R.W., 1972. Temperature and phytoplankton growth in the sea. Fish. Bull. 70, 1063–1085.

Kitano, M., Kurata, K., Kozuki, Y., Murakami, H., Yamasaki, T., Yoshida, H., Sasayama, H., 2003. Effects of deposit feeder *Stichopus japonicus* on algal bloom and organic matter contents of bottom sediments of the enclosed sea. Mar. Pollut. Bull. 47, 118–125.

Kitazawa, D., 2001. Numerical Analysis of the Impacts on Marine Ecosystem by a Very Large Floating Structure. The University of Tokyo (Ph.D Thesis. 373 pp in Japanese).

Kitazawa, D., Kumagai, M., Hasegawa, N., 2010. Effects of internal waves on dynamics of hypoxic waters in Lake Biwa. Journal of the Korean Society for Marine Environmental Engineering 13 (1), 30–42.

Kitazawa, D., Yang, J., 2012. Numerical analysis of water circulation and thermohaline structures in the Caspian Sea. J. Mar. Sci. Technol. 17, 168–180.

Li, J., Dong, S., Gao, Q., Wang, F., Tian, X., Zhang, S., 2014. Total organic carbon budget of integrated aquaculture system of sea cucumber *Apostichopus japonicus*, jellyfish *Rhopilema esculenta* and shrimp *Fenneropenaeus chinensis*. Aquac. Res. 45 (11), 1825–1831.

List, E., Gartrel, G., Winant, C., 1990. Diffusion and dispersion in coastal waters. J. Hydraul. Eng. 116, 1158–1179.

Mizumukai, K., Sato, T., Tabeta, S., Kitazawa, D., 2008. Numerical studies on ecological effects of artificial mixing of surface and bottom waters in density stratification in semi-enclosed bay and open sea. Ecol. Model. 214, 251–270.

Neori, A., Chopin, T., Troell, M., Buschmann, A.H., Kraemer, G.P., Halling, C., Shpigel, M., Yarish, C., 2004. Integrated aquaculture: rationale, evolution and state of the art emphasizing seaweed biofiltration in modern mariculture. Aquaculture 231, 361–391.

Okubo, A., 1975. Ocean diffusion diagrams. Deep-Sea Res. 18, 789–802.

Okubo, A., 1976. Remarks on the use of diffusion diagrams in modeling scale dependent diffusion. Deep-Sea Res. 23, 1213–1214.

Reid, G.K., 2011. Spatial modelling of integrated multi-trophic aquaculture (IMTA) shellfish. Bull. Aquac. Assoc. Can. 109, 39–44.

Reid, G.K., Liutkus, M., Robinson, S.M.C., Chopin, T.R., Blair, T., Lander, T., Mullen, J., Page, F., Moccia, R.D., 2009. A review of the biophysical properties of salmonid faeces: implications for aquaculture waste dispersal models and integrated multi-trophic aquaculture. Aquac. Res. 40, 257–273.

Ren, J.S., Stenton-Dozey, J., Plew, D.R., Fang, J., Gall, M., 2012. An ecosystem model for optimising production in integrated multitrophic aquaculture systems. Ecol. Model. 246, 34–46.

Ren, Y., Dong, S., Wang, F., Gao, Q., Tian, X., Liu, F., 2010. Sedimentation and sediment characteristics in sea cucumber *Apostichopus japonicus* (Selenka) culture ponds. Aquac. Res. 42, 14–21.

Sato, T., Tonoki, K., Tsuchiya, Y., 2006. Numerical and hydraulic simulations of effect of density current generators in semi-enclosed tidal bays. Coast. Eng. 53, 49–64.

Schlitzer, R., 2013. Ocean Data View. http://odv.awi.de.

Sfriso, A., Pavoni, B., Marcomini, A., 1989. Macroalgae and phytoplankton standing crops in the central Venice Lagoon: primary production and nutrient balance. Sci. Total Environ. 80, 139–159.

Solidoro, C., Pecenik, G., Pastres, R., Franco, D., Dejak, C., 1997. Modelling macroalgae (*Ulva rigida*) in the Venice lagoon: model structure identification and first parameters estimation. Ecol. Model. 94, 191–206.

Troell, M., Joyce, A., Chopin, T., Neori, A., Buschmann, A.H., Fang, J.G., 2009. Ecological engineering in aquaculture—potential for integrated multi-trophic aquaculture (IMTA) in marine offshore systems. Aquaculture 297, 1–9.

Uchida, T., Toda, S., Nakamura, O., Abo, K., Matsuyama, Y., Honjo, T., 1998. Initial site of *Gymnodinium mikimotoi* blooms in relation to the seawater exchange rate in Gokasho Bay, Japan. Plankton Biology and Ecology 45 (2), 129–137.

Yanagi, T., 2000. Coastal Oceanography (Ocean Science Research). first ed. Springer (ISBN-13:978-0792358954, 176 pp.).

Yokoyama, H., 2002. Impact of fish and pearl farming on the benthic environments in Gokasho Bay: evaluation from seasonal fluctuations of the macrobenthos. Fish. Sci. 68, 258–268.

Yokoyama, H., 2013. Growth and food source of the sea cucumber *Apostichopus japonicus* cultured below fish cages — potential for integrated multi-trophic aquaculture. Aquaculture 372–375, 28–38.

Yokoyama, H., Abo, K., Ishihi, Y., 2006. Quantifying aquaculture-derived organic matter in the sediment in and around a coastal fish farm using stable carbon and nitrogen isotope ratios. Aquaculture 254, 411–425.

Yokoyama, H., Ishihi, Y., 2010. Bioindicator and biofilter function of Ulva spp.(Chlorophyta) for dissolved inorganic nitrogen discharged from a coastal fish farm—potential role in integrated multi-trophic aquaculture. Aquaculture 310 (1), 74–83.

Yokoyama, H., Takashi, T., Ishihi, Y., Abo, K., 2009. Effects of restricted feeding on growth of red sea bream and sedimentation of aquaculture wastes. Aquaculture 286, 80–88.

Zhang, J., 2014. Numerical Analysis of Integrated Multi-Trophic Aquaculture for Biomitigation of Marine Ecosystem. The University of Tokyo (Ph.D Thesis. 223 pp).

Zhang, J., Kitazawa, D., Yang, C., 2015. A numerical modeling approach to support decision-making on design of integrated multitrophic aquaculture for efficiently mitigating aquatic waste. Mitig. Adapt. Strateg. Glob. Chang. 1–15.

Zhang, J., Kitazawa, D., 2015. Numerical analysis of particulate organic waste diffusion in an aquaculture area of Gokasho Bay, Japan. Mar. Pollut. Bull. 93 (1), 130–143.